Proceedings of the
9th Graz Brain-Computer Interface Conference 2024
10.3217/978-3-99161-014-4-091

DYNAMIC SUPPRESSION OF THE CORTEX THROUGH SYNCHRONISATION DURING BRAIN COMPUTER INTERFACING

F.E. Permezel[1], M.A. Jensen[2], D. Hermes[1,3], K.J. Miller[1,4]

[1]Department of Neurology, Mayo Clinic, MN, USA
[2]Department of Neurosurgery, Mayo Clinic, MN, USA
[3]Department of Biomedical Engineering, Mayo Clinic, MN, USA

E-mail: Permezel.fiona@mayo.edu

ABSTRACT:

This study investigates the neural dynamics of motor imagery and brain-computer interface (BCI) feedback through electrocorticography (ECoG). It focuses on how 12-20Hz rhythm entrainment with broadband power indicates cortical synchronization and suppression. The research examines 12-20Hz rhythm entrainment across rest and active phases in a motor task and BCI imagery feedback task. Using speech-associated broadband power increases in a speech motor area, a patient controlled a BCI system with word repetition imagery. The study examined broadband power shifts between rest and active task conditions, revealing increased power shifts in the speech motor area during the BCI imagery task as well as a unique activation in the dorsal motor area. Notably, it found increased broadband power to 12-20Hz rhythm coupling, indicating suppression of cortical activity, in the dorsal motor cortex during the BCI imagery feedback task's rest phase compared to the motor task rest phase, which may be suggestive of "cognitive control" over cortical suppression.

INTRODUCTION:

Recent advancements in brain-computer interface (BCI) technology have underscored the potential of motor imagery in enhancing motor skill acquisition and rehabilitation, particularly in individuals afflicted with neurological conditions [1-6]. The intricate neural mechanisms underlying these processes, including the activation of neocortical areas similar to those engaged during actual motor movements, have been illuminated through a variety of neuroimaging techniques, albeit with ongoing debates regarding the role of primary motor cortex in motor imagery [6-15]. Notwithstanding, the precision of electrocorticography (ECoG) in mapping somatotopic functions and capturing high-frequency cortical dynamics [16-22] has significantly advanced our understanding of these neural phenomena.

In parallel, the exploration of the beta rhythm in somatomotor regions has elucidated its inverse relationship with sensory processing and motor production, alongside its modulation in response to movement and motor imagery [18, 23-32]. These dynamics are often assessed using Phase Locking Value (PLV), a method well-documented by Lachaux et al. [47] for measuring the synchrony in brain signals, particularly in cortical-subcortical circuits which play a potential role in organizing somatomotor functions. This rhythm's involvement in cortical-subcortical circuits, particularly in relation to local neuronal activity and its potential role in organizing somatomotor function, has begun to be quantified, revealing a complex interplay of rhythm phase and broadband signal amplitude [33-39]. Miller [40] used ECoG electrodes in humans to study the phase-coupling of neuronal activity with the beta rhythm during finger movements. This study uncovered that broadband neuronal activity is phase-coupled with the beta rhythm, with this phase-coupling decreasing in amplitude during movement. The ECoG recording channels of greatest phase-coupling change with movement however, were not the same as those with the greatest beta activity change with movement. This study suggested that assessment of rhythm phase and broadband amplitude coupling may offer insights into the interplay of distinct brain rhythms and broadband amplitude during different activities. Building on these insights, our study leverages data from a participant engaged in motor and BCI feedback during motor imagery conditions collected previously by the Ojemann [41] group. We aim to dissect the nuanced shifts at specific electrode sites, with comparison between the motor vocalization and BCI imagery feedback conditions in i) broadband amplitude in response to action, ii) amplitude shifts of various rhythm frequencies in response to action, and iii) to delineate the changes with action and rest in the coupling between 12-20Hz rhythm phase and broadband amplitude. By examining these dynamics our work seeks to illuminate the underlying neural mechanisms of motor control and a BCI imagery feedback task, offering novel insights into their application in rehabilitative and BCI technologies.

CC BY
https://creativecommons.org/licenses/by/4.0/deed.en
This CC license does not apply to third party material and content noted otherwise.

Published by
Verlag der Technischen Universität Graz

10.3217/978-3-99161-014-4-091

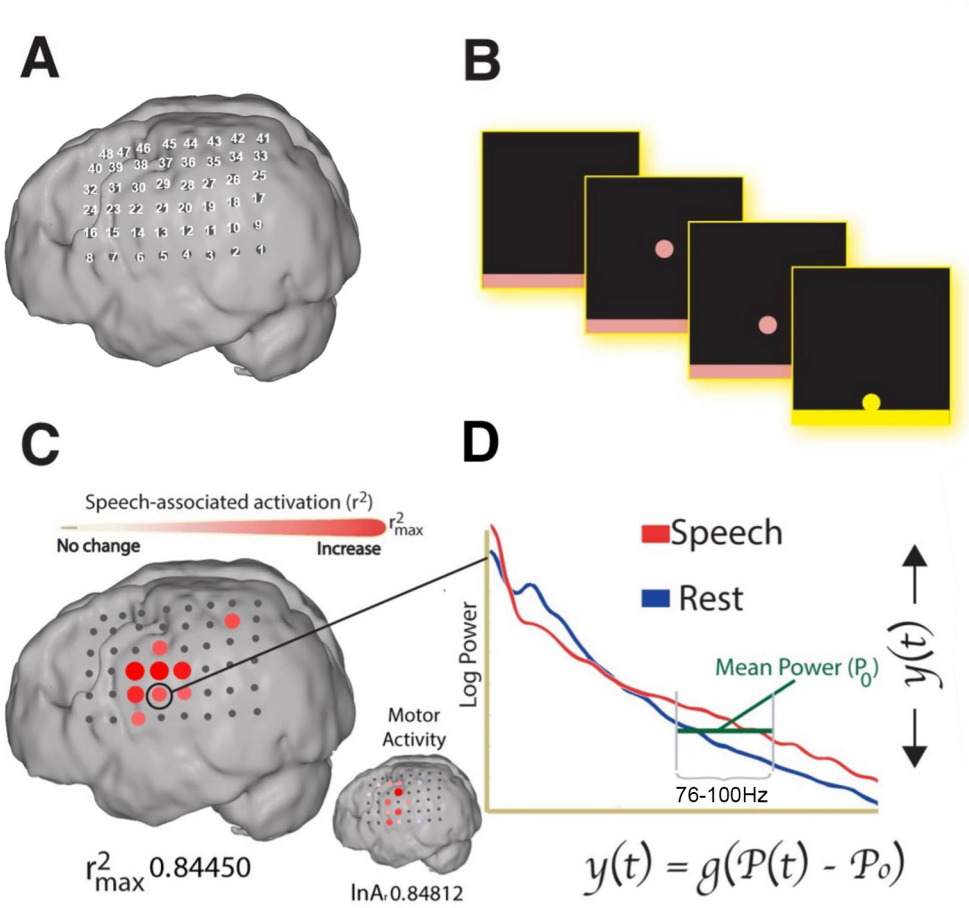

Figure 1: **BCI Imagery Feedback Task and Relation to Broadband Shift. (A)** Map of ECoG grid showing electrode positions. **(B)** Visual feedback of this broadband power change which causes moving of a dot on a screen in one direction. Reduction this broadband power increase will cause movement of the dot in the other direction. In the BCI imagery feedback experiement the patient is visually cued to try to move the dot in one direction or the other. **(C)** Dots represent significant ($p<0.05$ FDR corrected) broadband 76-100Hz power increase during BCI imagery feedback task active condition (motor imagery of saying „move“) compared to a rest condition. The smaller brain image shows the distribution of the same for the motor vocalization experiment. **(D)** The power spectra demonstrating the broadband increase with BCI imagery feedback compared to rest.

MATERIALS AND METHODS

Participant: The study included an epilepsy patient undergoing craniotomy for seizure localization, with informed consent under U.Washington IRB (#12193) approval. Data was downloaded from the ECoG Library database [42].

Stimulation: Electro-cortical mapping identified motor/speech cortices using 5–10 mA pulses.

Recordings: Signals from subdural platinum ECoG electrode arrays, with a total of 48 electrodes (Fig. 1.), were recorded at 1000Hz and processed for analysis.

Tasks: The patient performed the motor task of saying the word „move“, with multiple trials interspersed with rest periods. The patient then performed a BCI feedback task, where motor imagery of saying the word „move“ was utilized to move a cursor to a target, via ECoG recording detecting broadband power increase at an electrode chosen by the greatest broadband power increase in the motor task. The patient then is instructed to move the cursor away from the target (Fig. 1), which is actuated by reduction of this broadband increase at the specified electrode. It should be noted that the „rest“ condition in the feedback task was an „active rest“ task as the patient was deliberately attempting to move the cursor away from the „active vocalization imagery“ task.

Electrode Localization and Brain Mapping: Locations were estimated from x-rays and mapped to visualize activity distribution.

Data Analysis: A high-frequency broadband (HFB) ranging from 76–100 Hz was selected for the analysis. In brief this particular interval was chosen because it lies within this broad increase, avoids 60 Hz contamination, and matches the 25 Hz width of the low-frequency band (LFB), with further discussion on this

CC BY
https://creativecommons.org/licenses/by/4.0/deed.en
This CC license does not apply to third party material and content noted otherwise.

Published by
Verlag der Technischen Universität Graz

10.3217/978-3-99161-014-4-091

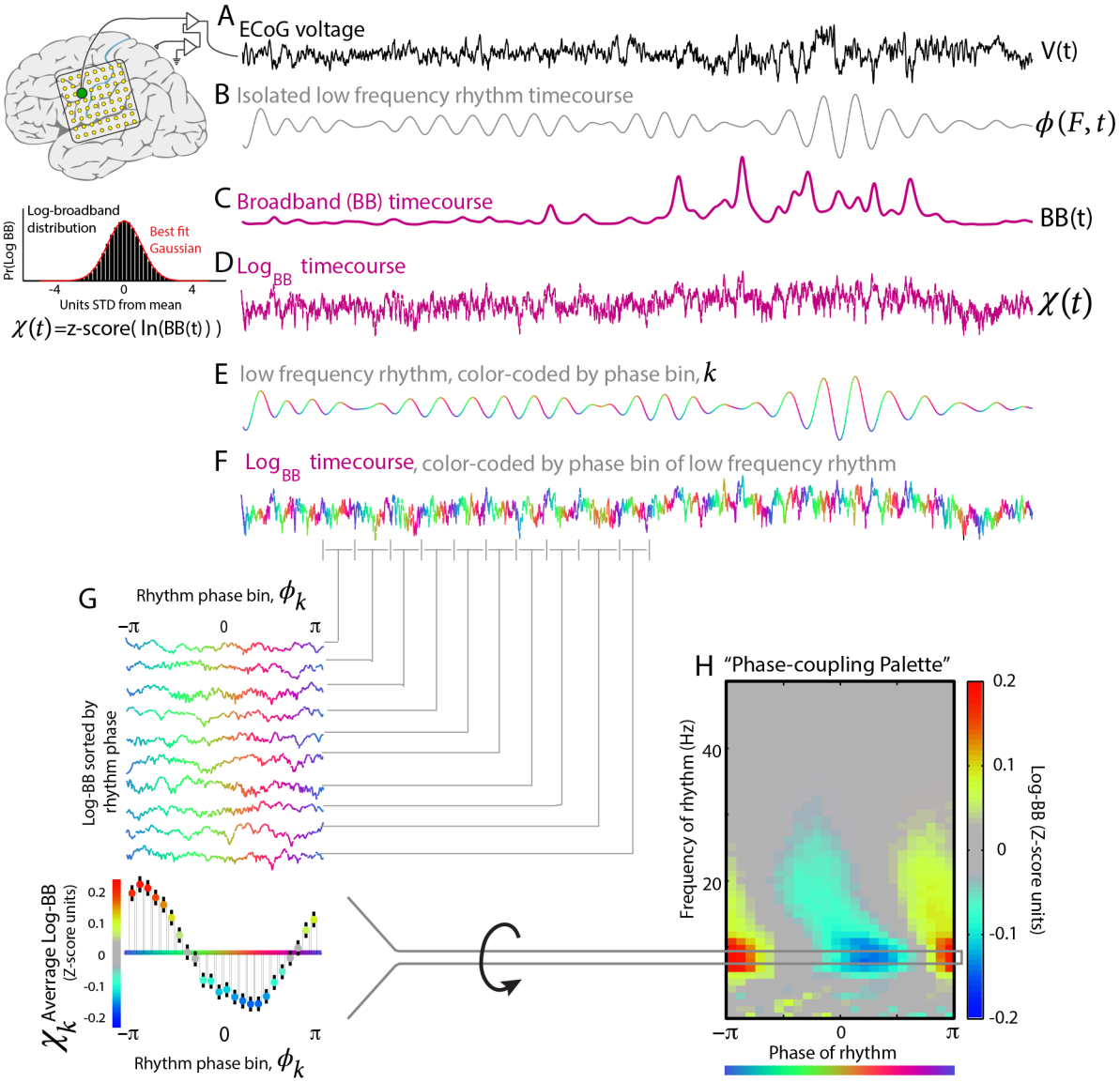

Figure 2: **Relation between broadband power and phase of ECoG rhythms. (A)** ECoG potential is measured from the cortex (green dot). **(B)** Example low frequency rhythm obtained by convolving ECoG with a simple Morlet wavelet. **(C)** Fluctuations in broadband power are also extracted from ECoG potential. **(D)** Log values of the time-dependent broadband have a normal distribution, so the z-scored log broadband timeseries is obtained. **(E)** The rhythm timeseries from B is shown color coded for instantaneous phase (relative to positivity peak of the potential). **(F)** The timeseries of the z-scored log of the broadband, color coded by the coincident phase of the low frequency rhythm. **(G)** The log-broadband signal is aligned with the phase of the low frequency rhythm (as color-coded). The average of the log-broadband amplitude is obtained for phase bins. Error bars denote 3 times the standard error of the mean (3*SEM) for each phase bin. This can be appreciated in one dimension as a row in the phase coupling palette (in H). **(H)** The full "Phase coupling palette" obtained by repeating the process detailed in E-G at each frequency from 1-50 Hz., showing modulation of broadband power with the full range of frequencies.

HFB frequency range selection outlined in prior studies [18]. In the patient's tests, which included verbalizing the word "move" and actual leg movement, only the verbal command was used for the feedback task. Therefore, comparisons were made between the periods of saying "move" and the rest periods immediately after, to account for the task-specific beta rebound following movement as noted by Pfurtscheller [31]. Cursor speed in the feedback task was updated every 40 ms, based on the power calculated from 79-95Hz and electrode numbers 13 and 22 over the preceding 280 ms.

1. Power Spectral Analysis: Power spectral density (PSD) of the signal was calculated for each epoch surrounding movement or imagery events.

$$(P(f,q) = \frac{1}{T}\left|\sum_{t=-T/2}^{T/2} V(t_q + t) \cdot H(t) \cdot e^{i2\pi ft}\right|^2)$$

CC BY
https://creativecommons.org/licenses/by/4.0/deed.en
This CC license does not apply to third party material and content noted otherwise.

Published by
Verlag der Technischen Universität Graz

10.3217/978-3-99161-014-4-091

Here (T) is the epoch duration, (t) is event duration, (f) is frequency, (q) is the event, $(V(t))$ is the electrode potential, (t_q) are event markers and $(H(t))$ is the Hann window function used to transform the time-domain data into frequency-domain representations, encompassing all frequencies during both rest and action phases.

2. High-Frequency Band Extraction (76-100 Hz): The averaged PSD for each movement or rest trial was normalized to the global mean across all trials. The power in the 76-100 Hz frequency range was extracted from the normalized PSD for each channel to focus on the high-frequency band (HFB) activity (Fig. 3A).

3. Phase-Amplitude Coupling (PAC) Analysis: Utilizing the Hilbert transform, the phase of the 12-20Hz rhythm and the amplitude of the HFB were used to generate phase-amplitude coupling metrics (Fig. 2):

$$(\tilde{V}(F,t) = r(F,t)e^{i\emptyset(F,t)})$$

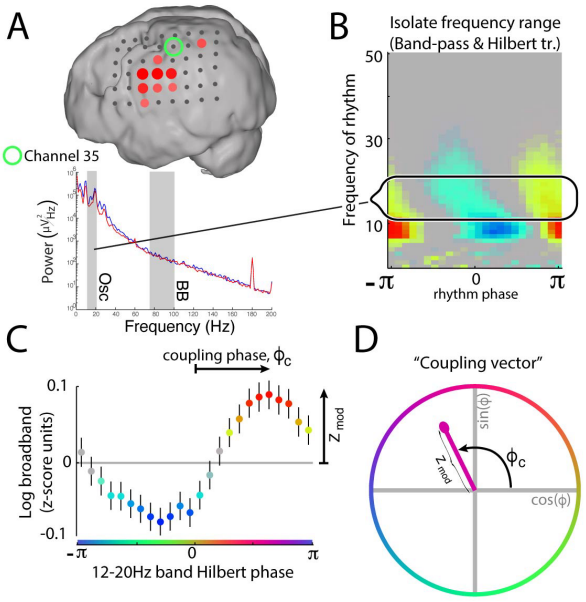

Figure 3: **Broadband and Phase Amplitude Coupling Palette at One Electrode. (A)** Demonstration of Channel 35 power spectra with regards to the broadband power change during BCI imagery feedback task active condition (motor imagery of saying „move“) compared to a rest condition. **(B)** Phase amplitude coupling palette at Channel 35 with the 12-20Hz frequency range circled. **(C & D)** Phase of rhythm depicted by color and angle on the complex plane.

Where $(\tilde{V}(F,t))$ is the complex PAC vector, for frequency range (F) = 12-20Hz at time (t). The ‘‘analytic amplitude’’ of the range (F) at time (t) is $(r(F,t))$ and the ‘‘phase’’ is $(\emptyset(F,t))$. Generation of metrics included constructing 'palettes' (Fig. 3) for each channel for each task to examine the relationship between phase and amplitude across frequencies. The coupling vector magnitude (Z_{mod}) and its preferred phase (w_c) are calculated as:

$$(Z_{mod}e^{iw_c} = \frac{1}{2K}\sum_k x_k e^{iw_k})$$

where (x_k) represents the average log-broadband amplitude in the k-th phase bin, $(w_k)$is the central phase of the k-th bin, and (K) is the total number of bins.

For assessing the distribution of phase-amplitude coupling values across trials (Fig. 4), the projected distribution is used:

$$(Z_{mod,q}(n) = Z_{mod}(n) \cdot \cos(w(n) - w_q))$$

where (n) is the trial number, $(w(n))$ is the preferred phase for the nth trial, and (w_q) is the preferred phase of the mean coupling vector for trials of type q, and (N) is this number of trials. The mean coupling vector is computed as:

$$(Z_{mod,q}e^{iw_q} = \frac{1}{N}\sum_n Z_{mod}(n)e^{iw(n)})$$

This method allows for the evaluation of the significance of phase-amplitude coupling by assessing the distribution of $(Z_{mod,q}(n))$ values.

4. Broadband and Rhythmic Amplitude Analysis: For each channel during rest and action phases, the broadband amplitude, the phase-amplitude coupling amplitude, and the amplitudes for rhythmic activities in the specified frequency band (12-20Hz) were calculated.

5. Statistical testing: Phase and amplitude of coupling vectors were calculated per trial for rest and active conditions for both BCI imagery feedback and motor tasks. For all conditions, each trial’s coupling vector was then projected to the mean phase angle across all trials.

Signed r^2 cross-correlation values at each channel were produced for each experimental condition (active vs rest) for each of broadband amplitude, phase-amplitude coupling amplitude and rhythmic amplitude.

A two-sample t-test was performed for each of broadband amplitude, phase-amplitude coupling amplitude and rhythmic amplitude and a significance p value calculated.

Channels with significant ($p<0.05$) r^2 values are demonstrated by colored circles on a 3D rendering of the patient’s brain with the diameter scaled to the magnitude of these r^2 values.

Power spectra of action vs rest conditions were plotted for motor vocalization and imagery feedback tasks.

Phase-amplitude coupling amplitudes (Zmod) for motor and feedback rest conditions were highlighted on a 3D rendering of the patient’s own brain with again only channels with Zmod with significant p values < 0.05 with FDR correction highlighted with channel dot size proportional to Zmod values. Dot color was related to the phase coupling angle $\emptyset_c$.

CC BY
https://creativecommons.org/licenses/by/4.0/deed.en
This CC license does not apply to third party material and content noted otherwise.

Published by
Verlag der Technischen Universität Graz

10.3217/978-3-99161-014-4-091

RESULTS

Comparison of broadband 76-100Hz power increase between the motor vocalization task vs. rest and the BCI imagery feedback task vs. rest (significant R values, $p<0.05$ after FDR correction) revealed a similar area of broadband increase, although the area with broadband increase extended over more channels in the speech area in the imagery feedback task (Fig. 3A). There was also a distinctly separate increase in one channel (37) in the dorsal motor area, only in the imagery feedback task (Fig. 3A).

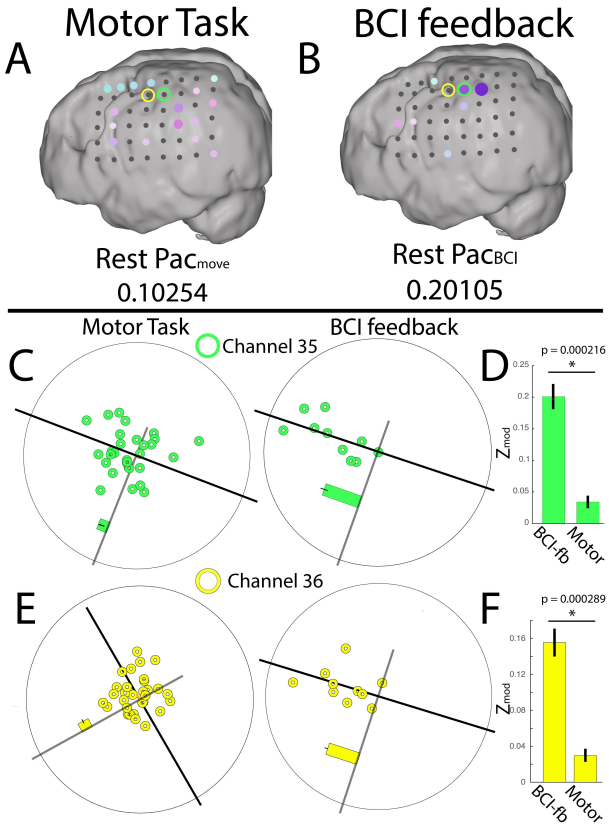

Figure 4: **Phase and Amplitude of the Coupling Vectors in the Rest Conditions. (A)** Shows the significant ($p < 0.05$ FDR corrected) values for the amplitude of the coupling vector (Zmod) of 12-20Hz to broadband power in the rest condition of the motor vocalization task. The size of the dot indicates the Zmod value, scaled to Zmod = 0.2. The color of the dot indicates the degree of phase. **(B)** The same as for A except for depicting the rest condition of the BCI imagery feedback task. **(C)** The phase (angle from center) and amplitude (distance from center) of coupling vectors for each trial (each dot) of the rest condition in the motor task and BCI feedback task at Channel 35. The black line parallel to the bar indicates the mean phase angle across trials. **(D)** The significant difference from a two-sample t-test (Bonferroni corrected $p<0.001$) between the mean Zmod (coupling amplitude) over trials between the BCI imagery feedback task and the vocalization motor task at Channel 35. **(E)** The same as (C) except for Channel 36. **(F)** the same as (D) except for Channel 36.

There was significant 12-20Hz rhythm decrease (significant R values, $p<0.05$ after FDR correction) around the face area of the primary motor and premotor cortex in the motor vocalization task, however there was no significant 12-20Hz shift in the imagery feedback task.

There was no significant increase or decrease in 12-20Hz to broadband coupling vector amplitude for task vs. rest for either the motor vocalization or imagery feedback task.

Examination of the amplitude and phase of the 12-20Hz to broadband coupling vectors for the rest condition revealed significantly increased coupling ($p<0.001$ Bonferroni adjusted for $p<0.05$) in channels 35 and 36 in the imagery feedback task at rest when compared to the motor vocalization task at rest. Channels 35 and 36 (Fig. 4) are in the dorsal motor area, distinctly separate from the speech area, and from the motor face area that demonstrated the 12-20Hz decrease with motor vocalization.

DISCUSSION

The finding of greater broadband 76-100Hz power increase over the speech area for task vs rest in the imagery feedback task compared to the motor vocalization task vs rest (Fig. 3A) is consistent with the results in the Ojemann group 2010 [41] study and other scientific investigations [43]. The heightened broadband power during BCI imagery feedback, relative to motor action, might stem from the initial selection of channel (13) for imagery feedback, based on its significant broadband power change during motor action. However, in our study, channel (13) was not the primary site of increased broadband power in the imagery feedback condition; instead, adjacent channels exhibited more substantial broadband increases compared to the motor vocalization task. This broader increase in broadband power during the BCI imagery feedback task, versus a motor task, suggests that the feedback mechanism itself might induce larger broadband shifts, a concept supported by Ushiba [44] and Neuper[45].

The single channel (37) of broadband power increase in the dorsal motor area (Fig. 3A) is difficult to explain during the motor vocalization imagery task and could be related to a motor association area activation [46].

The Ojemann group [41] found higher R values for low frequency (8-32Hz) power decrease in their imagery feedback task than their motor task. The current study found significant R values for 12-20Hz decrease with task only in the motor vocalization task and not the imagery feedback task. The reason for this difference in findings may be the different range of low-range frequencies tested. It may be that 20-32Hz is an important rhythm range for task related modulation in a vocalization imagery feedback task in the face motor area. In light of variations observed in correlation

CC BY
https://creativecommons.org/licenses/by/4.0/deed.en
This CC license does not apply to third party material and content noted otherwise.

Published by
Verlag der Technischen Universität Graz

10.3217/978-3-99161-014-4-091

between low-frequency power and task performance across studies, it is crucial to consider how different approaches to power estimation and normalization might influence findings. The methods employed in this study, detailed in the Methods section, follow established protocols but could still yield results that differ from those obtained using alternative analytical techniques. These differences might stem from how power spectra are normalized or from the spectral components that are emphasized or attenuated through different processing steps.

Miller in 2012 [40] demonstrated a broadband amplitude entrainment with 12-20Hz rhythm during rest periods (fixation) in the peri-central cortex. During finger movement this phase-entrainment was diminished or eliminated, suggesting the beta rhythm in the peri-central cortex to be a gating mechanism of motor function. The results of the present study did not demonstrate diminished entrainment of the broadband amplitude with 12-20Hz rhythm during motor vocalization or the active imagery phase of the feedback task. This may be related to the primary sites of motor activation in this study being outside of the dorsal peri-central cortex, as the task was motor vocalization and imaginary vocalization. There was however significantly higher broadband amplitude entrainment with a 12-20Hz rhythm in dorsal motor area channels (35 & 36) in the imagery feedback rest condition, when compared to the motor vocalization condition (Fig. 4). This relative dorsal motor cortex suppression during the "active relaxation" phase of the imagery feedback task may be evidence of unconscious suppression of motor cortex when attempting to moving a cursor in the opposite direction to that of the active imagery vocalization task. This suggests a degree of "cognitive control" over suppression of the cortex during the reinforced "rest" state of the BCI imager feedback experiment.

These results suggest a promising direction for future research in the BCI field, particularly in the use of phase-amplitude coupling (PAC) to assess deliberate cortical suppression during 'active rest' states. This approach may offer a novel method to electrophysiologically identify cognitive intentions, enhancing the responsiveness and adaptability of BCI systems. Further exploration into how variations in PAC correlate with specific cognitive tasks could lead to more intuitive interfaces that better align with user intent, potentially improving outcomes in therapeutic and rehabilitative applications.

REFERENCES

[1] Murphy, S.M., *Imagery interventions in sport.* Med Sci Sports Exerc, 1994. **26**(4): p. 486-94.
[2] Dijkerman, H.C., et al., *Does motor imagery training improve hand function in chronic stroke patients? A pilot study.* Clin Rehabil, 2004. **18**(5): p. 538-49.
[3] Page, S.J., P. Levine, and A. Leonard, *Mental practice in chronic stroke: results of a randomized, placebo-controlled trial.* Stroke, 2007. **38**(4): p. 1293-7.
[4] Alkadhi, H., et al., *What disconnection tells about motor imagery: evidence from paraplegic patients.* Cereb Cortex, 2005. **15**(2): p. 131-40.
[5] Sharma, N., V.M. Pomeroy, and J.C. Baron, *Motor imagery: a backdoor to the motor system after stroke?* Stroke, 2006. **37**(7): p. 1941-52.
[6] Hochberg, L.R., et al., *Neuronal ensemble control of prosthetic devices by a human with tetraplegia.* Nature, 2006. **442**(7099): p. 164-71.
[7] Naito, E., et al., *Internally simulated movement sensations during motor imagery activate cortical motor areas and the cerebellum.* Journal of Neuroscience, 2002. **22**(9): p. 3683.
[8] Jeannerod, M. and V. Frak, *Mental imaging of motor activity in humans.* Curr Opin Neurobiol, 1999. **9**(6): p. 735-9.
[9] de Lange, F.P., K. Roelofs, and I. Toni, *Motor imagery: A window into the mechanisms and alterations of the motor system.* Cortex, 2008. **44**(5): p. 494-506.
[10] Porro, C.A., et al., *Primary motor and sensory cortex activation during motor performance and motor imagery: a functional magnetic resonance imaging study.* J Neurosci, 1996. **16**(23): p. 7688-98.
[11] Roth, M., et al., *Possible involvement of primary motor cortex in mentally simulated movement: a functional magnetic resonance imaging study.* Neuroreport, 1996. **7**(7): p. 1280-4.
[12] Schnitzler, A., et al., *Involvement of primary motor cortex in motor imagery: a neuromagnetic study.* Neuroimage, 1997. **6**(3): p. 201-8.
[13] McFarland, D.J., et al., *Mu and beta rhythm topographies during motor imagery and actual movements.* Brain Topography, 2000. **12**(3): p. 177-186.
[14] Guillot, A., et al., *Brain activity during visual versus kinesthetic imagery: An fMRI study.* Human Brain Mapping, 2009. **30**: p. 2157.
[15] Hermes, D., et al., *Functional MRI-based identification of brain areas involved in motor imagery for implantable brain–computer interfaces.* Journal of Neural Engineering, 2011. **8**(2): p. 025007.
[16] Crone, N.E., et al., *Functional mapping of human sensorimotor cortex with electrocorticographic spectral analysis. II. Event-related synchronization in the gamma band.* Brain, 1998. **121 (Pt 12)**: p. 2301-15.
[17] Ball, T., et al., *Differential representation of arm movement direction.* Journal of Neural Engineering, 2009. **6**: p. 016006.
[18] Miller, K.J., et al., *Spectral changes in cortical surface potentials during motor movement.* J Neurosci, 2007. **27**(9): p. 2424-32.
[19] Aoki, F., et al., *Increased gamma-range activity in human sensorimotor cortex during performance of visuomotor tasks.* Clin Neurophysiol, 1999. **110**(3): p. 524-37.

CC BY
https://creativecommons.org/licenses/by/4.0/deed.en
This CC license does not apply to third party material and content noted otherwise.

Published by
Verlag der Technischen Universität Graz

10.3217/978-3-99161-014-4-091

[20] Kubánek, J., et al., *Decoding flexion of individual fingers using electrocorticographic signals in humans.* Journal of Neural Engineering, 2009. **6**: p. 066001.
[21] Miller, K.J., et al., *Decoupling the Cortical Power Spectrum Reveals Real-Time Representation of Individual Finger Movements in Humans.* Journal of Neuroscience, 2009. **29**(10): p. 3132.
[22] Manning, J.R., et al., *Broadband shifts in LFP power spectra are correlated with single-neuron spiking in humans.* Journal of Neuroscience, 2009. **29**(43): p. 13613–13620.
[23] Jasper, H.H., *Electrical activity of the brain.* Annual Review of Physiology, 1941. **3**(1): p. 377-398.
[24] Miller, F.R., G.W. Stavraky, and G.A. Woonton, *Effects of eserine, acetylcholine and atropine on the electrocorticogram.* Journal of Neurophysiology, 1940. **3**(2): p. 131.
[25] Bartley, S.H. and P. Heinbecker, *The response of the sensorimotor cortex to stimulation of a peripheral nerve.* American Journal of Physiology--Legacy Content, 1937. **121**(1): p. 21.
[26] Penfield, W., *Mechanisms of voluntary movement.* Brain, 1954. **77**(1): p. 1.
[27] Jasper, H. and W. Penfield, *Electrocorticograms in man: effect of voluntary movement upon the electrical activity of the precentral gyrus.* European Archives of Psychiatry and Clinical Neuroscience, 1949. **183**(1): p. 163-174.
[28] Bates, J.A., *Electrical activity of the cortex accompanying movement.* J Physiol, 1951. **113**(2-3): p. 240-57.
[29] Jasper, H.H. and H.L. Andrews, *Brain potentials and voluntary muscle activity in man.* Journal of Neurophysiology, 1938. **1**(2): p. 87.
[30] Crone, N.E., et al., *Functional mapping of human sensorimotor cortex with electrocorticographic spectral analysis. I. Alpha and beta event-related desynchronization.* Brain, 1998. **121 (Pt 12)**: p. 2271-99.
[31] Pfurtscheller, G., *Event-Related Desynchronization (ERD) and Event Related Synchronization (ERS)*. Electroencephalography: Basic Principles, Clinical Applications and Related Fields, ed. E. Niedermeyer and F. Lopes da Silva. 1999, Baltimore: Williams and Wilkins. 958-967.
[32] Miller, K.J., et al., *Cortical activity during motor execution, motor imagery, and imagery-based online feedback.* Proceedings of the National Academy of Sciences, 2010. **108**(9): p. 4430-4435.
[33] Murthy, V.N. and E.E. Fetz, *Coherent 25- to 35-Hz oscillations in the sensorimotor cortex of awake behaving monkeys.* Proc Natl Acad Sci U S A, 1992. **89**(12): p. 5670-4.
[34] Murthy, V.N. and E.E. Fetz, *Synchronization of neurons during local field potential oscillations in sensorimotor cortex of awake monkeys.* J Neurophysiol, 1996. **76**(6): p. 3968-82.
[35] Reimer, J. and N.G. Hatsopoulos, *Periodicity and evoked responses in motor cortex.* J Neurosci, 2010. **30**(34): p. 11506-15.
[36] Manning, J.R., et al., *Broadband shifts in local field potential power spectra are correlated with single-neuron spiking in humans.* Journal of Neuroscience, 2009. **29**(43): p. 13613.
[37] Miller, K.J., *Broadband Spectral Change: Evidence for a Macroscale Correlate of Population Firing Rate?* Journal of Neuroscience, 2010. **30**(19): p. 6477.
[38] Miller, K.J., et al., *Power-law scaling in the brain surface electric potential.* PLoS computational biology, 2009. **5**(12): p. e1000609.
[39] Ray, S. and J.H. Maunsell, *Different origins of gamma rhythm and high-gamma activity in macaque visual cortex.* PLoS Biol, 2011. **9**(4): p. e1000610.
[40] Miller, K.J., et al., *Human motor cortical activity is selectively phase-entrained on underlying rhythms.* PLoS Comput Biol, 2012. **8**(9): p. e1002655.
[41] Miller, K.J., et al., *Cortical activity during motor execution, motor imagery, and imagery-based online feedback.* Proc Natl Acad Sci U S A, 2010. **107**(9): p. 4430-5.
[42] Miller, K.J., *A library of human electrocorticographic data and analyses.* Nature Human Behaviour, 2019. **3**(11): p. 1225-1235.
[43] Wolpaw, J.R., J.D.R. Millán, and N.F. Ramsey, *Brain-computer interfaces: Definitions and principles.* Handb Clin Neurol, 2020. **168**: p. 15-23.
[44] Ushiba, J., et al. *Feeling of Bodily Congruence to Visual Stimuli Improves Motor Imagery Based Brain-Computer Interface Control*. in *Converging Clinical and Engineering Research on Neurorehabilitation II*. 2017. Cham: Springer International Publishing.
[45] Neuper, C., et al., *Motor imagery and action observation: Modulation of sensorimotor brain rhythms during mental control of a brain–computer interface.* Clinical Neurophysiology, 2009. **120**(2): p. 239-247.
[46] Jensen, M.A., et al., *A motor association area in the depths of the central sulcus.* Nature Neuroscience, 2023. **26**(7): p. 1165-1169.
[47] Lachaux, J. P., et al., *Measuring phase synchrony in brain signals.* Human brain mapping, 1999. **8**(4), 194–208.

CC BY
https://creativecommons.org/licenses/by/4.0/deed.en
This CC license does not apply to third party material and content noted otherwise.

Published by
Verlag der Technischen Universität Graz